JACS
JOURNAL OF THE AMERICAN CHEMICAL SOCIETY
Article
pubs.acs.org/JACS

Synthesis and Structural Features of Quadruple Helicenes: Highly Distorted π Systems Enabled by Accumulation of Helical Repulsions

Takao Fujikawa,[†] Yasutomo Segawa,*[,†,‡] and Kenichiro Itami*[,†,‡,§]

[†]Graduate School of Science, [‡]JST, ERATO, Itami Molecular Nanocarbon Project, and [§]Institute of Transformative Bio-Molecules (WPI-ITbM), Nagoya University, Nagoya 464-8602, Japan

Supporting Information

ABSTRACT: Quadruple helicenes, bearing dithia[6]helicene and [5]helicene substructures, were prepared by a well-controlled Scholl reaction. The 4-fold helicity provides 9 stereoisomers including 4 pairs of enantiomers and 1 meso isomer. Among them, differently distorted structures of a propeller-shaped isomer (**QH-A**) and a saddle-shaped isomer (**QH-B**) were unambiguously determined by X-ray crystallography. Especially in the latter isomer, a proper accumulation of repulsions on the helical substructures twisted the naphthalene core to the limit (69.5°), the highest degree of twisting deformation per benzene unit (35.3° at the most). Photophysical and electrochemical studies showed a broadened HOMO−LUMO gap and a HOMO of **QH-B** lying lower compared to those of **QH-A**. These results together with the density functional theory (DFT) calculations have clearly demonstrated the electronic state dependency on the molecular geometry. Additionally, kinetic studies of the isomerization between these isomers using ^{1}H NMR, circular dichroism, and DFT calculations shed light on the interconversion pathways among the stereoisomers. The height of barriers in the inversion of a certain helical substructure may be affected by the neighboring helical substructures.

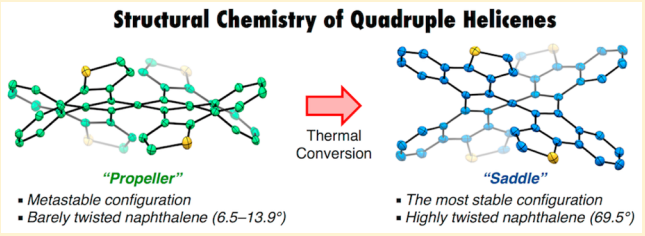

INTRODUCTION

A deviation from planarity strongly perturbs the properties of π systems, which has made the chemistry of nonplanar aromatics an ever-growing research field.[1] In nonplanar aromatic chemistry, two approaches are known to achieve a deformation of π systems. One is the endoskeletal approach in which a nonhexagonal ring is included inside the hexagonal skeleton (e.g., [*n*]circulenes).[2] The other is the exoskeletal approach with tightly bridged transannular connections or steric hindrance stemming from the crowdedness of atoms (e.g., cyclophanes or helicenes).[3,4] The creation of such nonplanar π systems and the development of new synthetic methods have attracted much interest to understand the limits and possibilities of π systems.

Twisted aromatics are one of the nonplanar π systems; they show chiroptical properties and dynamic behavior because of their helical molecular geometries.[5] Profound twisting deformation has been achieved exclusively by using the exoskeletal approach and evaluated by the end-to-end twist angle of the core π system. Pascal's twisted pentacene is the most illustrious example, with a total twist angle of 144° (Figure 1, left bottom).[5c] Besides such twisted acenes, Shinokubo and co-workers also reported the synthesis of a twisted porphyrin tetramer with the "total" twist angle of ca. 300°.[6] Like these examples, total twisting occurs as long as the core π system is elongated. Then, another viewpoint of twisting deformation arises: twist angle per a ring of specific number. As well-documented in all the studies on twisted acenes, aromatic annulation provides a strong repulsive effect on the core π system compared to that of bulky substituents. Thus, a twisted pentacene records the largest twist angle of 30° per a single benzene unit as the outcome of 4-fold benzannulation in addition to sixfold phenylation. Kamikawa recently reported a double [5]helicene exhibiting the same degree of twisting due to the steric hindrance of 4-fold annulation of naphthalene rings on its central naphthalene core (Figure 1, right bottom).[7]

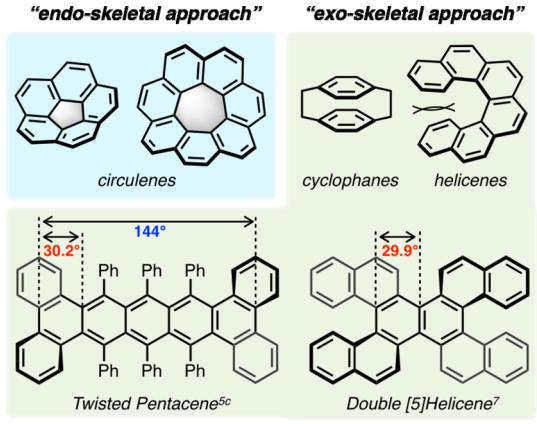

Figure 1. Nonplanar π systems achieved by endoskeletal and exoskeletal approaches. The maximum twist angles per benzene unit (red) and the total twist angles (blue) are shown for twisted aromatics.

Received: February 4, 2016
Published: February 26, 2016

DOI: 10.1021/jacs.6b01303
J. Am. Chem. Soc. 2016, 138, 3587−3595

In this article, we describe the unprecedented twisted nature of quadruple helicenes as a new milestone of twisted π systems. The arrangement of dithia[6]helicene[8] and [5]helicene substructures around a naphthalene core generates 4-fold helical π systems (Figure 2). Because of the proper

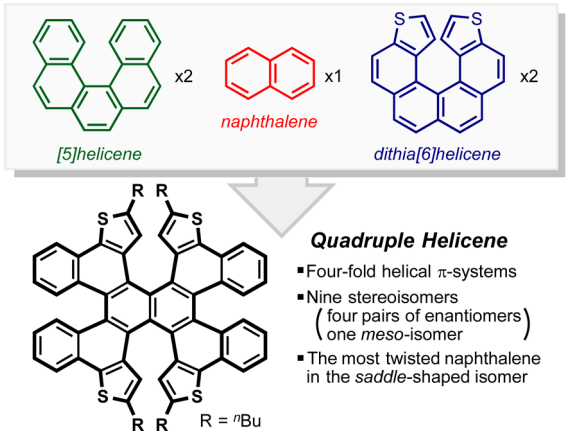

Figure 2. Quadruple helicene.

accumulation of repulsions on helical substructures, the most severely twisted benzene rings of up to 35° as well as a naphthalene core near 70° were achieved as a saddle-shaped isomer. A comparison with propeller-shaped isomer also showed the dependence of electronic structure on the molecular geometry of π systems.

RESULTS AND DISCUSSION

Synthesis, Isomerization, and Racemization. The quadruple helicenes (**QHs**) were unexpectedly obtained during the synthesis of the analogous compounds of a previously reported π-extended double helicene (Scheme 1).[9] At the

Scheme 1. Synthetic Scheme of Previously Reported π-Extended Double Helicene

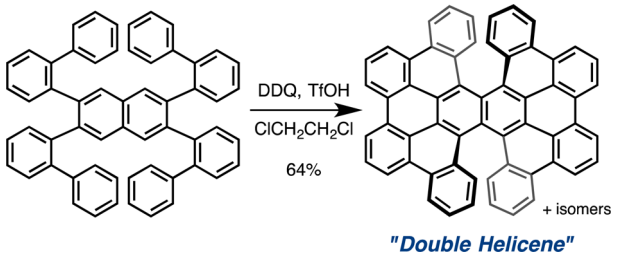

beginning, for the synthesis of an thiophene-containing double helicene congener **6**, compound **5** was synthesized (Scheme 2). The nucleophilic substitution of α-lithiated *n*-butylthiophene to 1,2-dibromobenzene (**1**) afforded 2-(2-bromophenyl)-5-butylthiophene (**2**) in 97% yield.[10] Successive lithiation of **2** and treatment with trimethyl borate produced boronic acid **3**, which was used in the following step without purification. Next, the 4-fold Suzuki–Miyaura coupling reaction of **3** with **4** using $Pd_2(dba)_3$, 2-dicyclohexylphosphino-2′,6′-dimethoxybiphenyl (SPhos), and Cs_2CO_3 provided **5** in 72% yield.[11] With compound **5** in hand, the Scholl reaction (cyclodehydrogenation) was investigated under various conditions initially aiming at having **6**.[12] However, when the conditions including DDQ/acid systems used in the previous synthesis of double helicene[9] were screened, an incompletely cyclized product **QH-A** was obtained in 57% yield instead of the expected double helicene **6** by the treatment of Mo(V) chloride in the presence of molecular sieves. The molecular sieves probably scavenged the hydrochloric acid generated in situ, thus controlling the oxidizing power of Mo(V) chloride.[13] Moreover, a quantitative thermal conversion of **QH-A** to another isomer **QH-B** was accomplished by reacting for 2 days at 80 °C in 1,1,2,2-tetrachloroethane-d_2. This result indicates that **QH-A** is a kinetic product in the Scholl reaction which can be converted into a more stable isomer **QH-B** and that the barrier to the isomerization is sufficiently high to handle **QH-A** at room temperature without isomerization.

Thus-obtained **QHs** should have two substructures, dithia[6]helicene and [5]helicene, in a fully conjugated manner. The ^{1}H NMR analysis showed a simple spectrum with one singlet, two doublets, and two triplets for each isomer. Notably, the singlet peaks corresponding to the hydrogen atoms at the end of the inner helix of dithia[6]helicene substructures in **QH-A** (δ 6.14 ppm) showed a large downfield shift after the conversion to **QH-B** (δ 7.29 ppm), indicating a significant deshielding upon structural change (Figure 3).

Considering the 4-fold helicity of **QH**, we can depict nine stereoisomers including four pairs of enantiomers and one meso isomer (five diastereomers in total, Figure 4). Therefore, the X-ray crystallography of both the products was carried out to determine their stereochemistry. **QH-A** was characterized as a racemate of (*P*,*P*)-(*P*,*P*)-**QH** and (*M*,*M*)-(*M*,*M*)-**QH** (helicity notation in the right bottom of Figure 4); all the helical substructures possess identical helicity, forming a propeller-shaped molecular geometry (vide infra). **QH-B** was also characterized as a racemate of (*P*,*P*)-(*M*,*M*)-**QH** and (*M*,*M*)-(*P*,*P*)-**QH**; the two different helical substructures possess opposite helicity, forming a saddle-shaped molecular geometry. Both the structures determined here have a higher symmetry of D_2 than those of C_2 for **QH-C** and **QH-D** or C_i for **QH-E**. This is also consistent with their simple ^{1}H NMR spectra.

The presence of chiral π systems resulting from the combination of helicity in **QHs** motivated us to separate their enantiomers. First, optical resolution of **QH-A** was carried out using means of HPLC equipped with a COSMOSIL cholester column. The specific optical rotation $[\alpha]_D^{20}$ of the faster eluting peak (>99% *ee*, Figure S1; (+)-**QH-A**) was determined to be + 496 (*c* 0.10, CH_2Cl_2). In contrast, because the complete chiral separation of **QH-B** by HPLC failed, we intended to conduct the thermal conversion of enantiopure **QH-A** to the corresponding enantiopure **QH-B** without racemization (Scheme 3). By heating a toluene solution of (+)-**QH-A** at 80 °C for 2 days, an enantiopure product (+)-**QH-B** with a specific rotation $[\alpha]_D^{20}$ of + 426 (*c* 0.0496, CH_2Cl_2) was successfully obtained.[14] These $[\alpha]_D^{20}$ values were rather small compared to those of single helicenes, which are generally above 1000 as the absolute value.[15] The progress in the racemization of **QH-B** was also confirmed by heating a 1,2,4-trichlorobenzene solution of (+)-**QH-B** at an elevated temperature of above 185 °C (Figure S2).

Structures. Single-crystal X-ray structure analyses were carried out using the racemic single crystals of **QH-A** recrystallized from *n*-pentane solution and **QH-B** recrystallized from a solution of chloroform and 2-propanol. The crystal of **QH-A** contained two crystallographically independent molecules (**QH-A-1** colored in red and **QH-A-2** colored in green in Figures 5a,b).

DOI: 10.1021/jacs.6b01303
J. Am. Chem. Soc. 2016, 138, 3587–3595

Scheme 2. Synthesis of Quadruple Helicenes (QHs)[a]

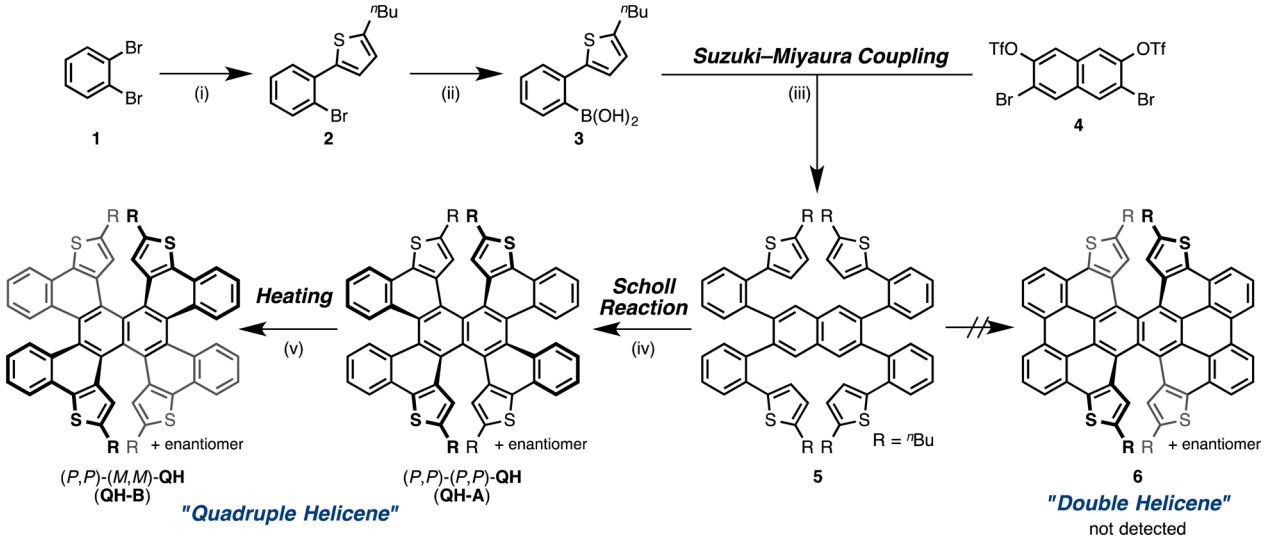

[a]Reaction conditions: (i) 2-butylthiophene (1.5 equiv), *n*-BuLi (1.5 equiv), THF, −40 °C, 1 h; then, **1** (1 equiv), RT, 20 h (97% yield); (ii) *n*-BuLi (1.05 equiv), THF, −78 °C, 1 h; then, trimethoxyborane (3 equiv), RT, 16 h (**3** was used in the next step without purification); (iii) **3** (ca. 10 equiv), $Pd_2(dba)_3{\cdot}CHCl_3$ (10 mol %), SPhos (20 mol %), Cs_2CO_3 (10 equiv), toluene/H_2O (2:1), 80 °C, 3 days (72% yield); (iv) $MoCl_5$ (10 equiv), MS4A, CH_2Cl_2 (5 mM), 0 °C, 2 h (57% yield); (v) 1,1,2,2-tetrachloroethane-d_2, 80 °C, 2 days (quant., NMR yield using Me_2SO_2 as the internal standard).

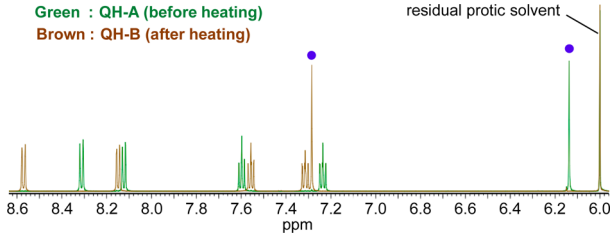

Figure 3. ^{1}H NMR spectra of **QHs** in 1,1,2,2-tetrachloroethane-d_2. The spectra of **QH-A** (before heating) and **QH-B** (after heating) are colored green and brown, respectively. Singlet peaks of the hydrogens at the end of inner helix of dithia[6]helicene substructures are marked by purple circles.

The most notable structural difference between two isomers is the end-to-end twist of central naphthalene cores. For **QH-A**, the twist angle ranges from 6.5° (**QH-A-2**) to 13.9° (**QH-A-1**). Conversely, **QH-B** showed a profound twist angle reaching 69.5° (Figure 5c). To the best of our knowledge, this twisting deformation of a naphthalene core is the highest among various nonplanar π systems when converted to those of a single benzene unit (35.3 and 34.2°).[5,7] Clearly, the origin of this exceptional distortion can be attributed to a proper accumulation of repulsions on helical substructures. As shown by the studies on twisted acenes developed by the group of Pascal,[16] the rigidness caused by annulation provides a large repulsive effect, forcing the core π system to form highly twisted geometries. In the case of **QH-B**, all the repulsions on helical substructures cause the same directional distortion to the central naphthalene, resulting in such an extremely twisted structure.

A large distortion of **QH-B** was also reflected in the splay angles of helical substructures, herein defined as the selected dihedral angles of four inner carbon atoms (Figure 5d). Although the splay angles of 23.7° in [5]helicene substructures and 51.4° in dithia[6]helicene substructures on average for **QH-A-1** and 29.5 and 46.0° on average for **QH-A-2** are comparable to those in pristine [5]helicene (27.9° in the X-ray structure)[17] and dithia[6]helicene (46.4° in the optimized structure), respectively, **QH-B** showed larger splay angles of 43.7 and 62.6°. This structural difference in helical distortion may be maintained in the solution phase because of the significant disparity of the chemical shift of inner singlet hydrogen atoms between the two isomers (Figure 3) indicating more compressed dithia[6]helicene substructures of **QH-A**. The inner hydrogen atoms in **QH-A** are properly located over the polycyclic aromatic system and therefore have a great shielding effect. To support this assumption, we carried out the NMR calculations of optimized structures and imperfect structures by removing two biaryl units and replacing the inner hydrogen atoms with dummy atoms. The difference in the estimated shielding constants ($\Delta\delta$ = 1.39) of dummy atoms is in good agreement with the difference in the estimated chemical shifts of inner hydrogen atoms ($\Delta\delta$ = 1.13); thus, we excluded the possibility of the ring current deterioration of annulated thiophene rings (Figure S7).

Another characteristic difference between two isomers is the dihedral angles of four selected carbon atoms in their central naphthalene skeletons. The naphthalene cores of **QH-A** showed relatively small dihedral angles at the edge of naphthalene cores (8.4(2) and 11.3(2)° for **QH-A-1** and 13.4(2) and 14.8(2)° for **QH-A-2**) and at the center (23.9(2) and 26.0(2)° for **QH-A-1** and 20.6(2) and 21.3(2)° for **QH-A-2**) compared to those of **QH-B** (32.5(3) and 35.6(3)° at the edge and 42.5(3) and 42.7(3)° at the center). In contrast to these substantial differences in the dihedral angles, a negligible difference was observed in the bond lengths of naphthalene rings between two isomers (Figure S5). Hence, only a slightly enhanced bond alternation upon the conversion from **QH-A** to **QH-B** was estimated from the value of the harmonic oscillator model of aromaticity (HOMA)[18] of two independent rings (avg HOMA = 0.369 for **QH-A** and avg HOMA = 0.537 for **QH-B**).

DOI: 10.1021/jacs.6b01303
J. Am. Chem. Soc. 2016, 138, 3587−3595

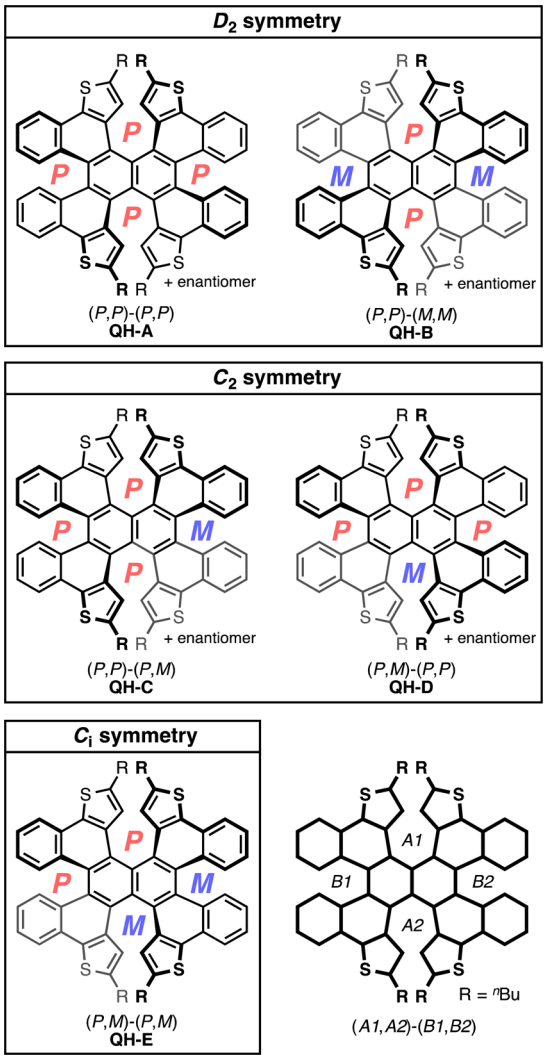

Figure 4. Nine stereoisomers of **QH**.

Scheme 3. Thermal Isomerization from (+)-QH-A to (+)-QH-B and Racemization of (+)-QH-B

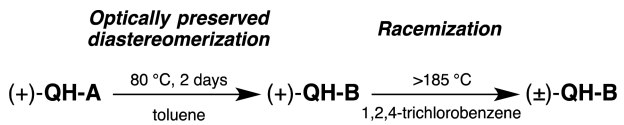

Electronic Structures of QH-A and QH-B. *Photophysical Properties.* The UV−vis absorption and fluorescence spectra of **QH-A** and **QH-B** clearly showed the difference in the molecular geometries, affecting electronic structures (Figure 6a). The propeller-shaped geometry (**QH-A**) resulted in a weak shoulderlike absorption band at ∼520 nm in addition to a weak absorption maximum at 459 nm and an intense absorption maximum at 405 nm (ε = 5.9 × 10^4). In comparison, the saddle-shaped geometry (**QH-B**) afforded a similar but blue-shifted spectrum with a weak shoulderlike absorption band at ∼495 nm in addition to a weak broad absorption band in the region 400−480 nm and an intense absorption at 381 nm (ε = 7.7 × 10^4). A blueshift was observed in the fluorescence spectra in the same manner, producing fluorescence maxima at 536 and 570 nm (Φ_F = 0.017) for **QH-A** and at 514 nm for **QH-B** (Φ_F = 0.11).

Time-Dependent Density Functional Theory Study. Time-dependent density functional theory (TD-DFT) calculations (B3LYP/6-31G(d)) confirmed the spectral change between **QH-A** and **QH-B**.[19] Both the absorptions of shoulder bands at ∼500 nm (S_1) and intense absorptions around 400 nm (S_4) were assigned to the HOMO−1 → LUMO/HOMO → LUMO +1 transitions, and the weak absorptions at ∼450 nm (S_2) were assigned to the HOMO → LUMO/HOMO−1 → LUMO+1 transitions (Figure 6c). Notably, computations showed that the energy levels of HOMO−1/HOMO and LUMO/LUMO+1 were reversed upon the change in geometry affording different frontier orbitals in each isomer. These inversions of frontier orbitals can be attributed to the difference in connectivity of π conjugation along the shorter axis of the naphthalene core. The larger dihedral angle at the edge of central naphthalene in **QH-B** (Figure 5) probably disrupts the π conjugation along the path from one thiophene ring to the other (i.e., along the *p*-dithiophenylbenzene skeleton) and lowers the energies of orbitals involving this conjugation such as the HOMO and LUMO of **QH-A**.

Electrochemistry. The energy level difference between the HOMOs of **QH-A** (−4.94 eV) and **QH-B** (−5.09 eV) estimated from DFT calculations was confirmed electrochemically (Figure 7). The cyclic voltammetry of **QH-A** showed reversible two-step oxidation wave with the half-wave potential $E_{1/2}$ of 0.48 and 0.87 V (vs FcH/FcH^+) and that of **QH-B** showed reversible oxidation wave with the half-wave potential $E_{1/2}$ of 0.64 V (vs FcH/FcH^+). The second oxidation wave of **QH-B** was not observed reversibly, which may be due to the instability of the oxidized product. A difference of 0.16 V in the first oxidation potentials of the two isomers is consistent with the calculated results.

Circular Dichroism. The circular dichroism (CD) spectra of (+)-**QH-A** exhibited negative Cotton effects in the region 370−530 nm in response to the extinction coefficient of absorption spectra, and an intense signal with a positive Cotton effect at ∼330 nm (Figure 6b). In contrast, the CD spectra of (+)-**QH-B** in the longer wavelength region showed Cotton effects almost opposite to those of (+)-**QH-A** except for the negative signal at ∼445 nm. The signal corresponding to the intense signal at ∼330 nm in the spectra of (+)-**QH-A** became so weakened and unclear in the case of (+)-**QH-B**. Because of the good agreement of the experimental CD spectra with the simulated spectra obtained from the TD-DFT calculations (Figure S6), (+)-**QH-A** was assigned as (*P*,*P*)-(*P*,*P*)-**QH**, and (+)-**QH-B** was assigned as (*P*,*P*)-(*M*,*M*)-**QH**. Inevitably, (−)-**QH-A**, which eluted slower and showed CD spectra mirror-image to that of (+)-**QH-A**, was assigned as (*M*,*M*)-(*M*,*M*)-**QH** (Figure S7).

Geometry-Dependent Electronic Structure. Several multihelical π systems have plural electronic structures due to the presence of diastereomers. Only a few articles, however, mentioned the dependence of electronic structure on the molecular geometry on the basis of the experimental results.[9,20] In this case, we successfully uncovered the geometry dependence of HOMO−LUMO gaps, HOMO energy levels, frontier orbitals, fluorescence quantum yields, and chiroptical properties between **QH-A** and **QH-B** from the photophysical and electrochemical analyses in addition to DFT studies.

Kinetics of the Interconversion Pathway among QHs. In association with any transitions between the five diastereomers, one of the four helical substructures of **QHs** inverts. On the basis of this inversion law, the interconversion

DOI: 10.1021/jacs.6b01303
J. Am. Chem. Soc. 2016, 138, 3587−3595

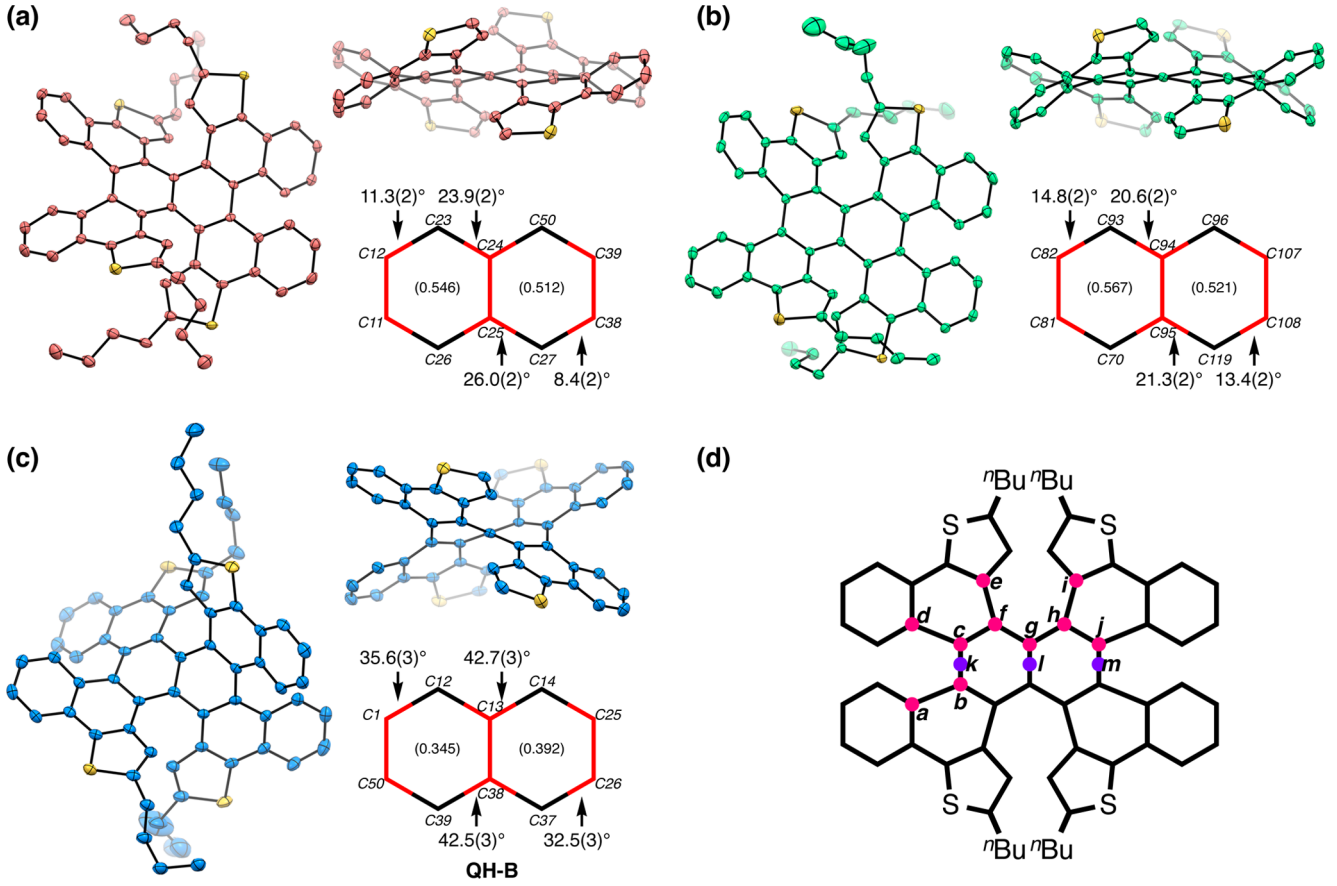

Figure 5. X-ray structures and their naphthalene cores with HOMA values (in parentheses) and dihedral angles (colored in red) of (a) **QH-A-1** ((*P*,*P*)-(*P*,*P*), red), (b) **QH-A-2** ((*P*,*P*)-(*P*,*P*), green)), and (c) **QH-B** ((*P*,*P*)-(*M*,*M*), blue). ORTEP drawings are shown with 50% probability; the hydrogen atoms and the minor part of the disordered moieties are omitted for clarity. The *n*-butyl groups are also omitted for clarity in side views. (d) Selected carbon atoms and centroids for the estimation of end-to-end twist angles (C(c)−C(k)−C(m)−C(j)), twist angles per benzene unit (C(c)−C(k)−C(l)−C(g) and C(g)−C(l)−C(m)−C(j)), and splay angels of helical substructures (C(a)−C(b)−C(c)−C(d) for [5]helicene substructures and C(e)−C(f)−C(h)−C(i) for dithia[6]helicene substructures). See Figures S3−S5 for detailed structural parameters.

pathway was investigated theoretically (B3LYP/6-31G(d)). The *n*-butyl groups of **QHs** were replaced with methyl groups to simplify the calculations. As a consequence, six transition states with face-to-face oriented terminal aromatic rings of helical substructures were found (Figure 8).[21] This indicates that **QH-A** isomerizes to the most thermodynamically stable **QH-B** (stable by 8.1 kcal·mol^{-1}) after the temporal isomerization to **QH-C** (Figure 9a). Along this conversion, only the inversions of [5]helicene substructures occur; the calculated activation free energy from **QH-A** to $\mathbf{TS}_{\mathbf{A-C}}$ ($\Delta G^{\ddagger}$ = 29.0 kcal·mol^{-1}) is higher than that from **QH-C** to $\mathbf{TS}_{\mathbf{B-C}}$ ($\Delta G^{\ddagger}$ = 25.5 kcal·mol^{-1}). Thus, it can be inferred that the former step is the rate-determining step (RDS).[22]

The kinetics of the isomerization from **QH-A** to **QH-B** were studied experimentally by monitoring the decreasing integration of **QH-A** in the ^{1}H NMR spectra in 1,1,2,2-tetrachloroethane-d_2. As simulated theoretically, the ignorable emergence of the integration of tentatively assigned **QH-C** supported the predicted location of the RDS (Figure S10). Because of the substantial disparity in thermodynamic stabilities, the reverse conversion could be neglected. The first-order rate constants k_c (s^{-1}) of the forward conversion at various temperatures were estimated using the following equation:

$$\ln([\mathbf{QH\text{-}A}]_t/[\mathbf{QH\text{-}A}]_0) = -k_c t \quad (1)$$

where $[\mathbf{QH\text{-}A}]_0$ is the initial ratio of the integration of **QH-A** to the sum of the integration of **QH-A** and **QH-B** and $[\mathbf{QH\text{-}A}]_t$ is the ratio of the integration of **QH-A** at a certain time *t* during the conversion (Figure 10a). Using these data, an Eyring plot was constructed using the following equation:

$$\ln(k/T) = -\Delta H^{\ddagger}/RT + [\ln(k_B/h) + \Delta S^{\ddagger}/R] \quad (2)$$

where *R* is the gas constant, *T* is the measured temperature, *A* is the frequency factor, $\Delta H^{\ddagger}$ is the activation enthalpy, k_B is the Boltzmann constant, *h* is the Planck constant, and $\Delta S^{\ddagger}$ is the activation entropy. This plot provided the activation parameters $\Delta H^{\ddagger}$ = 28.6 kcal·mol^{-1}, $\Delta S^{\ddagger}$ = 2.6 cal·mol^{-1}·K^{-1}, and $\Delta G^{\ddagger}$ = 27.8 kcal·mol^{-1} at 298 K (Figure S11). A higher barrier to this conversion than that of the inversion of [5]helicene ($\Delta G^{\ddagger}$ = 24.1 kcal·mol^{-1})[23] may reflect the presence of additional repulsion from the neighboring dithia[6]helicene substructure at the transition state.

The interconversion pathway of **QHs** (Figure 8) indicates that any one of the barriers obtained with the inversion of dithia[6]helicene substructures can be estimated by monitoring the racemization progress of the enantiopure **QH-B**, necessarily including the inversions of both the helicene substructures. The most plausible racemization process is the path: *ent*-**QH-B** → *ent*-**QH-C** → **QH-E** (*meso*) → *rac*-**QH-C** → *rac*-**QH-B**, where the RDS is the step from *ent*-**QH-B** to $\mathbf{TS}_{\mathbf{C-E}}$ ($\Delta G^{\ddagger}$ = 35.5 kcal·

DOI: 10.1021/jacs.6b01303
J. Am. Chem. Soc. 2016, 138, 3587−3595

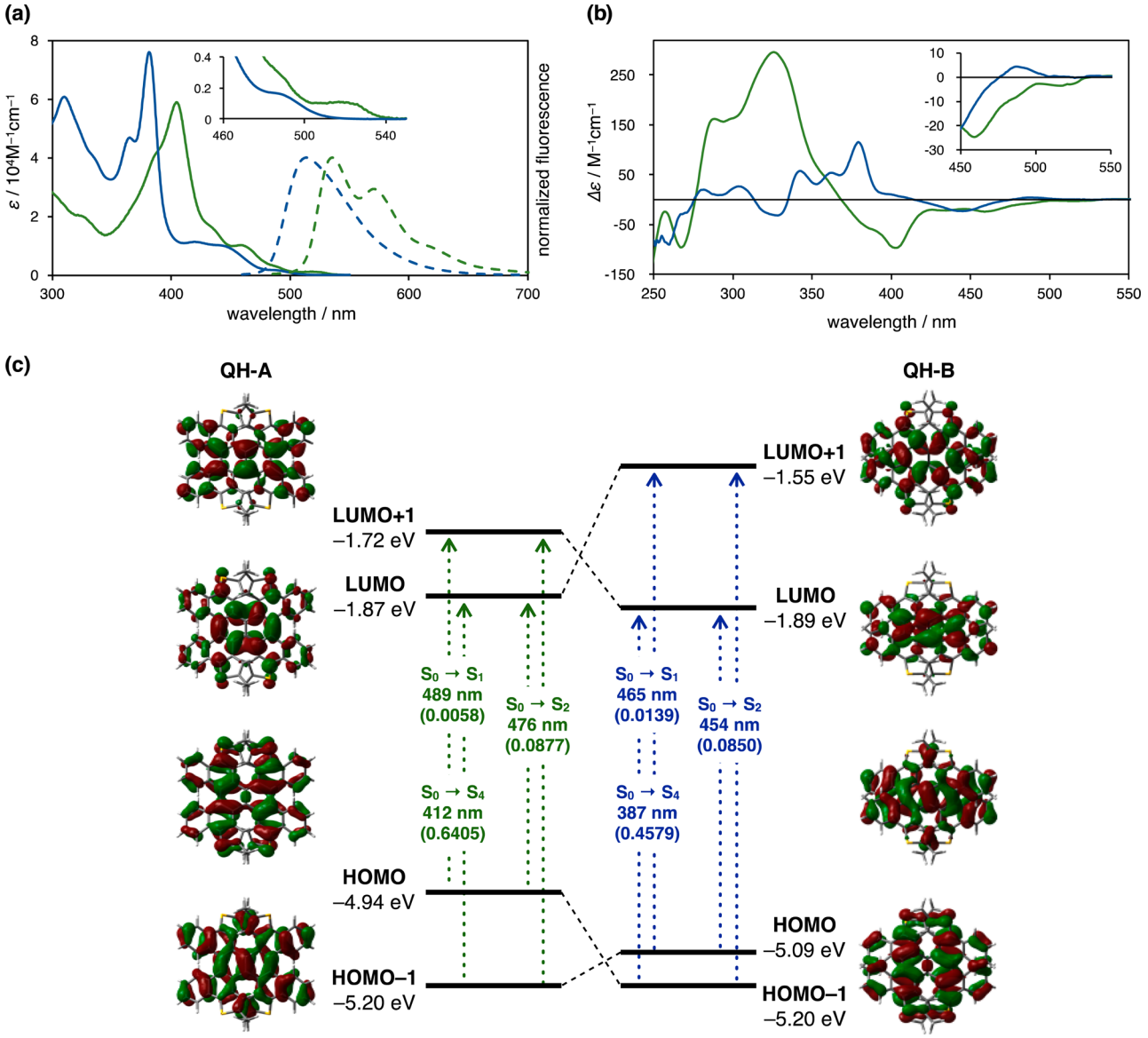

Figure 6. (a) UV–vis absorption spectra (solid lines) and fluorescence spectra (broken lines) of **QH-A** (green) and **QH-B** (blue) in dichloromethane. (b) Experimental CD spectra of **QH-A**$_{first}$ (green; assigned to (*P*,*P*)-(*P*,*P*)-**QH**) and **QH-B**$_{second}$ (blue; assigned to (*P*,*P*)-(*M*,*M*)-**QH**). (c) Energy diagrams of **QH-A** and **QH-B** calculated at the B3LYP/6-31G(d) level of theory. Excitation energies were computed by TD-DFT calculations at the same level. Values in parentheses represent oscillator strengths (*f*).

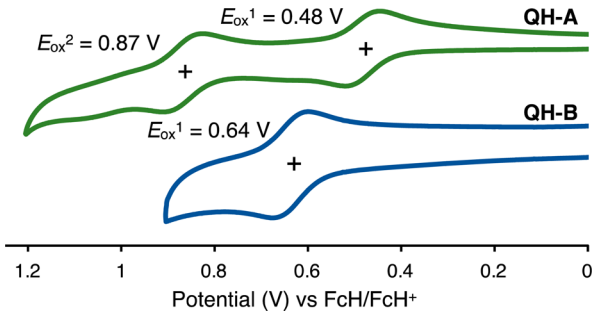

Figure 7. Cyclic voltammograms of **QH-A** (green) and **QH-B** (blue) in dichloromethane containing 100 mM of $TBAPF_6$ at scan rate of 0.1 V s^{-1}. FcH = ferrocene.

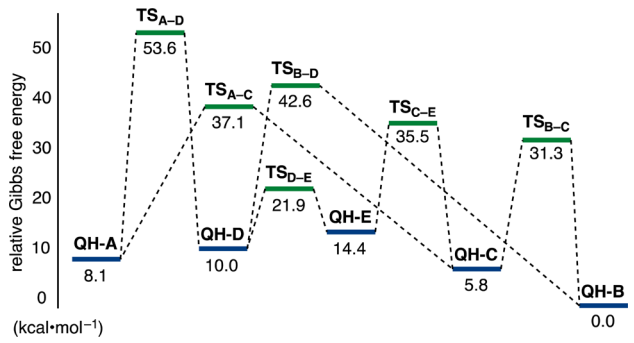

Figure 8. Interconversion pathway among **QH-A**–**QH-E** calculated at the B3LYP/6-31G(d) level.

mol^{-1}; Figure 9b).[21] This process differs from the usual racemization of single helicenes[23] because **QH-B** loses its initial chiral information upon conversion to the achiral intermediate **QH-E**, whereas the initial chirality information is maintained as the opposite helicity in the case of single helicenes. This

DOI: 10.1021/jacs.6b01303
J. Am. Chem. Soc. 2016, 138, 3587–3595

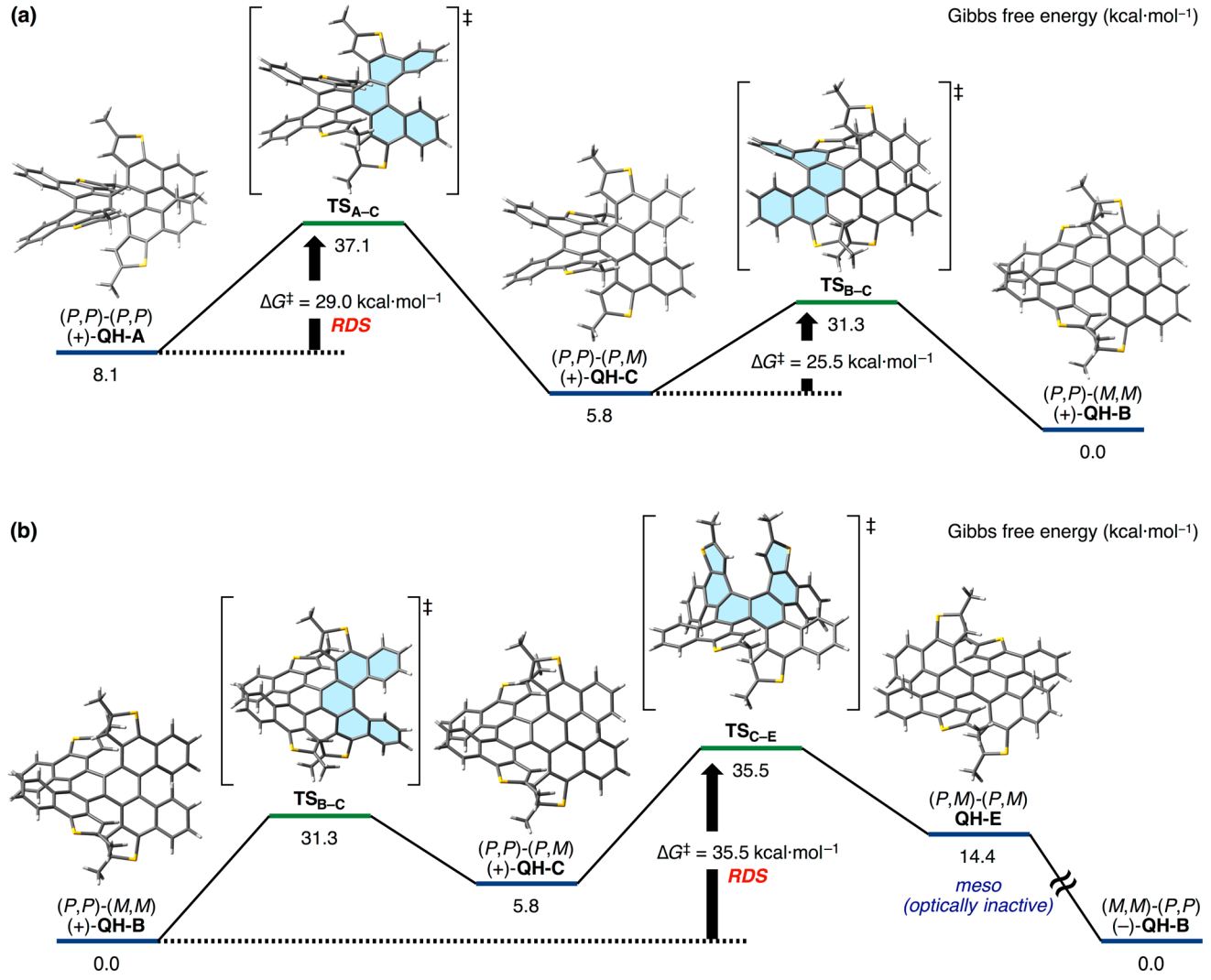

Figure 9. Structures of intermediates and transition states during (a) the most plausible diastereomerization from (*P*,*P*)-(*P*,*P*)-**QH** ((+)-**QH-A**) to (*P*,*P*)-(*M*,*M*)-**QH** ((+)-**QH-B**) and (b) the most plausible enantiomerization from (*P*,*P*)-(*M*,*M*)-**QH** ((+)-**QH-B**) to (*M*,*M*)-(*P*,*P*)-**QH** ((−)-**QH-B**). (The energy diagram of the process from **QH-E** to (−)-**QH-B** is equal to that of the process from **QH-E** to (+)-**QH-B**; therefore, it was omitted here.) Helical substructures that invert in transition states are highlighted in blue.

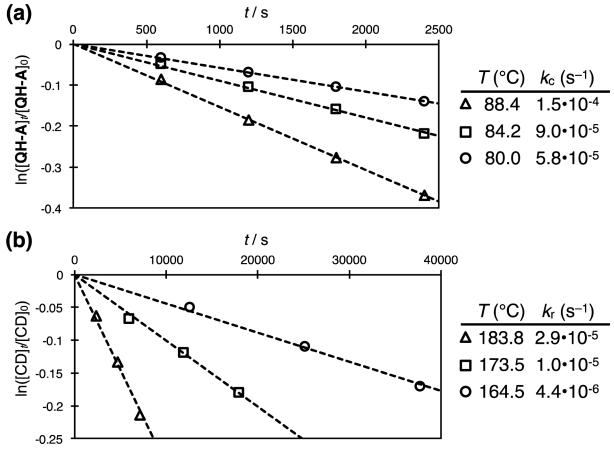

Figure 10. (a) Plots of the decreasing integration of **QH-A** in the ^{1}H NMR spectra in 1,1,2,2-tetrachloroethane-d_2 upon heating at 80.0, 84.2, and 88.4 °C. (b) Plots of the decreasing ellipticity at 382 nm in the CD spectra of enantioenriched **QH-B** in 1,2,4-trichlorobenzene upon heating at 164.5, 173.5, and 183.8 °C.

indicates that the rate constant of racemization (k_r) is equal to that of the isomerization (k_i) from **QH-B** to **QH-E**.

Because **QH-B** was the most thermodynamically stable isomer and the ratio of other metastable isomers were vanishingly small during the thermal interconversion, kinetics of the racemization of enantioenriched **QH-B** were studied experimentally by monitoring the decreasing ellipticity in the CD spectra in 1,2,4-trichlorobenzene. The first-order rate constants k_r (s^{-1}) at various temperatures were estimated using the following equation:

$$\ln([\mathrm{CD}]_t/[\mathrm{CD}]_0) = -k_r t \quad (3)$$

where $[\mathrm{CD}]_0$ is the initial ellipticity of enantioenriched **QH-B** and $[\mathrm{CD}]_t$ is the ellipticity at a certain time t during the racemization (Figure 10b). Using these data, the Eyring plot was constructed using eq 2. This plot provided the activation parameters $\Delta H^{\ddagger}$ = 37.8 kcal·mol^{-1}, $\Delta S^{\ddagger}$ = 2.6 cal·mol^{-1}·K^{-1}, and $\Delta G^{\ddagger}$ = 37.1 kcal·mol^{-1} at 298 K (Figure S13). The barrier to this racemization was comparable to that of [6]helicene ($\Delta G^{\ddagger}_{300\ \mathrm{K}}$ = 36.2 kcal·mol^{-1}).[24] Unlike the case of the conversion from **QH-A** to **QH-B**, none of the additional

DOI: 10.1021/jacs.6b01303
J. Am. Chem. Soc. 2016, 138, 3587−3595

repulsion from the neighboring [5]helicene substructures exists at the transition state; therefore, we obtained a barrier slightly lower than the calculated barrier of the corresponding single dithia[6]helicene ($\Delta G^{\ddagger}$ = 39.3 kcal·mol^{-1}, Figure S15).

CONCLUSIONS

We have reported the synthesis and structural features of quadruple helicenes. The presence of 4-fold helicity resulted in 9 stereoisomers including 4 pairs of enantiomers and 1 meso isomer. Interestingly, the significant distortion of saddle-shaped isomer (**QH-B**), derived from the proper accumulation of repulsions on helical substructures, had the highest degree of twisting deformation per benzene unit (35.3° at the most). The photophysical and electrochemical studies showed the electronic structures of **QH-A** (propeller-shaped isomer) and **QH-B**, providing information for the better understanding of the dependence of electronic structure on the molecular geometry. The experimental and theoretical kinetic studies also showed the complicated interconversion pathway among the stereoisomers. As demonstrated here and in our previous study,[9] the well-controlled Scholl reaction of naphthalene derivatives with four biaryl units has proven to be a powerful strategy for the generation of distorted π systems with multihelicity. We believe that the multifaceted study of highly distorted multihelicenes will not only lay the groundwork in the growing realm of nonplanar π systems but also lead to the development of new functional materials.

ASSOCIATED CONTENT

Supporting Information

The Supporting Information is available free of charge on the ACS Publications website at DOI: 10.1021/jacs.6b01303.

Experimental procedures, characterization of data for all new compounds, and crystallographic data of **QH-A** and **QH-B**. (PDF)

Crystallographic information file for **QH-A** and **QH-B**. (CIF)

AUTHOR INFORMATION

Corresponding Authors

*E-mail: ysegawa@nagoya-u.jp.

*E-mail: itami@chem.nagoya-u.ac.jp.

Notes

The authors declare no competing financial interest.

ACKNOWLEDGMENTS

This work was supported by the ERATO program from JST (K.I.). T.F. thanks IGER Program in Green Natural Sciences, Nagoya University, and JSPS fellowships for young scientists. Calculations were carried out using the resources of the Research Center for Computational Science, Okazaki, Japan. Institute of Transformative Bio-Molecules is supported by the World Premier International Research Center (WPI) Initiative, Japan.

REFERENCES

(1) Reviews on nonplanar π systems: (a) Rieger, R.; Müllen, K. *J. Phys. Org. Chem.* **2010**, *23*, 315. (b) Dodziuk, H. *Strained Hydrocarbons: Beyond the van't Hoff and Le Bel Hypothesis*; Wiley-VCH: Weinheim, 2009. (c) Harvey, R. G. *Polycyclic Aromatic Hydrocarbons*; Wiley-VCH: New York, 1997. (d) Pascal, R. A., Jr. *Chem. Rev.* **2006**, *106*, 4809. (e) Tsefrikas, V. M.; Scott, L. T. *Chem. Rev.* **2006**, *106*, 4868. (f) Wu, Y.-T.; Siegel, J. S. *Chem. Rev.* **2006**, *106*, 4843.

(2) Circulenes: (a) Barth, W. E.; Lawton, R. G. *J. Am. Chem. Soc.* **1966**, *88*, 380. (b) Yamamoto, K.; Harada, T.; Okamoto, Y.; Chikamatsu, H.; Nakazaki, M.; Kai, Y.; Nakao, T.; Tanaka, M.; Harada, S.; Kasai, N. *J. Am. Chem. Soc.* **1988**, *110*, 3578. (c) Bharat; Bhola, R.; Bally, T.; Valente, A.; Cyrański, M. K.; Dobrzycki, Ł.; Spain, S. M.; Rempała, P.; Chin, M. R.; King, B. T. *Angew. Chem., Int. Ed.* **2010**, *49*, 399. (d) Feng, C.-N.; Kuo, M.-Y.; Wu, Y.-T. *Angew. Chem., Int. Ed.* **2013**, *52*, 7791. (e) Sakamoto, Y.; Suzuki, T. *J. Am. Chem. Soc.* **2013**, *135*, 14074.

(3) Reviews on cyclophanes: (a) Gleiter, R.; Hopf, H. *Modern Cyclophane Chemistry*; Wiley-VCH, Weinheim, 2004. (b) Kane, V. V.; De Wolf, W. H.; Bickelhaupt, F. *Tetrahedron* **1994**, *50*, 4575.

(4) Reviews on helicenes: (a) Gingras, M. *Chem. Soc. Rev.* **2013**, *42*, 968. (b) Gingras, M.; Félix, G.; Peresutti, R. *Chem. Soc. Rev.* **2013**, *42*, 1007. (c) Gingras, M. *Chem. Soc. Rev.* **2013**, *42*, 1051. (d) Shen, Y.; Chen, C.-F. *Chem. Rev.* **2012**, *112*, 1463.

(5) Twisted π systems: (a) Wang, K. K. *Top. Curr. Chem.* **2012**, *349*, 31. (b) ref 1d. (c) Lu, J.; Ho, D. M.; Vogelaar, N. J.; Kraml, C. M.; Pascal, R. A., Jr. *J. Am. Chem. Soc.* **2004**, *126*, 11168. (d) Schuster, I. I.; Craciun, L.; Ho, D. M.; Pascal, R. A., Jr. *Tetrahedron* **2002**, *58*, 8875. (e) Qiao, X.; Ho, D. M.; Pascal, R. A., Jr. *Angew. Chem., Int. Ed. Engl.* **1997**, *36*, 1531. (f) Qiao, X.; Padula, M. A.; Ho, D. M.; Vogelaar, N. J.; Schutt, C. E.; Pascal, R. A., Jr. *J. Am. Chem. Soc.* **1996**, *118*, 741. (g) Smyth, N.; Van Engen, D.; Pascal, R. A., Jr. *J. Org. Chem.* **1990**, *55*, 1937. (h) Pascal, R. A., Jr.; McMillan, W. D.; Van Engen, D.; Eason, R. G. *J. Am. Chem. Soc.* **1987**, *109*, 4660.

(6) Ito, S.; Hiroto, S.; Lee, S.; Son, M.; Hisaki, I.; Yoshida, T.; Kim, D.; Kobayashi, N.; Shinokubo, H. *J. Am. Chem. Soc.* **2015**, *137*, 142.

(7) Kashihara, H.; Asada, T.; Kamikawa, K. *Chem. - Eur. J.* **2015**, *21*, 6523.

(8) Thiahelicenes: (a) Waghray, D.; de Vet, C.; Karypidou, K.; Dehaen, W. *J. Org. Chem.* **2013**, *78*, 11147. (b) Pieters, G.; Gaucher, A.; Marque, S.; Maurel, F.; Lesot, P.; Prim, D. *J. Org. Chem.* **2010**, *75*, 2096. (c) Dopper, J. H.; Oudman, D.; Wynberg, H. *J. Am. Chem. Soc.* **1973**, *95*, 3692.

(9) Fujikawa, T.; Segawa, Y.; Itami, K. *J. Am. Chem. Soc.* **2015**, *137*, 7763.

(10) Becht, J.-M.; Ngouela, S.; Wagner, A.; Mioskowski, C. *Tetrahedron* **2004**, *60*, 6853.

(11) (a) Shinamura, S.; Osaka, I.; Miyazaki, E.; Nakao, A.; Yamagishi, M.; Takeya, J.; Takimiya, K. *J. Am. Chem. Soc.* **2011**, *133*, 5024. (b) Cooke, R. G.; Johnson, B. L.; Owen, W. R. *Aust. J. Chem.* **1960**, *13*, 256.

(12) Review of Scholl reaction: Grzybowski, M.; Skonieczny, K.; Butenschön, H.; Gryko, D. T. *Angew. Chem., Int. Ed.* **2013**, *52*, 9900.

(13) Kramer, B.; Fröhlich, R.; Waldvogel, S. R. *Eur. J. Org. Chem.* **2003**, *2003*, 3549.

(14) The optical purity of (+)-**QH-B** most plausibly drops when **QH-C** is converted into **QH-E**. From the DFT calculations, the $\Delta G^{\ddagger}$ values from **QH-C** to $\mathbf{TS}_{\mathbf{B-C}}$ and $\mathbf{TS}_{\mathbf{C-E}}$ were 25.5 and 29.7 kcal·mol^{-1}, respectively (Figure S14). This difference in the activation free energies by 4.2 kcal·mol^{-1} would result in a rate constant of the former process 1200-fold larger than that of the latter process at 298 K (estimated using the equation $k = (k_B T/h)\exp(-\Delta G^{\ddagger}/RT)$). Experimentally, the optical purity of (+)-**QH-B** was checked by HPLC (Figure S2).

(15) Nakai, Y.; Mori, T.; Inoue, Y. *J. Phys. Chem. A* **2012**, *116*, 7372.

(16) Twist angles per benzene unit of twisted acenes are 19−25° for decaphenylanthracene, 22−29° for octaphenyldibenzotetracene, and 27−30° for hexaphenyltetrabenzopentacene (refs 5c,e,f).

(17) Kuroda, R. *J. Chem. Soc., Perkin Trans. 2* **1982**, 789.

(18) (a) Krygowski, T. M.; Cyrański, M. K. *Chem. Rev.* **2001**, *101*, 1385. (b) Krygowski, T. M. *J. Chem. Inf. Model.* **1993**, *33*, 70. (c) Kruszewski, J.; Krygowski, T. M. *Tetrahedron Lett.* **1972**, *13*, 3839.

(19) Five diastereomers of QHs (**QH-A**−**QH-E**) optimized by B3LYP/6-31G(d) level of theory represented energetic local minima.

DOI: 10.1021/jacs.6b01303
J. Am. Chem. Soc. 2016, 138, 3587−3595

Optimized structures of **QH-A** and **QH-B** reproduced X-ray structures well. See Table S2.
(20) (a) Liu, X.; Yu, P.; Xu, L.; Yang, J.; Shi, J.; Wang, Z.; Cheng, Y.; Wang, H. *J. Org. Chem.* **2013**, *78*, 6316. (b) Luo, J.; Xu, X.; Mao, R.; Miao, Q. *J. Am. Chem. Soc.* **2012**, *134*, 13796. (c) Lütke Eversloh, C. L.; Liu, Z.; Müller, B.; Stangl, M.; Li, C.; Müllen, K. *Org. Lett.* **2011**, *13*, 5528. (d) Peña, D.; Cobas, A.; Pérez, D.; Guitián, E.; Castedo, L. *Org. Lett.* **2000**, *2*, 1629.
(21) (a) Grimme, S.; Peyerimhoff, S. D. *Chem. Phys.* **1996**, *204*, 411. (b) Janke, R. H.; Haufe, G.; Würthwein, E.-U.; Borkent, J. H. *J. Am. Chem. Soc.* **1996**, *118*, 6031.
(22) See Figure S14 for other calculation results of interconversion pathway at the M06-2X/6-31G(d) and BMK/6-31G(d) level of theory.
(23) Goedicke, C.; Stegemeyer, H. *Tetrahedron Lett.* **1970**, *11*, 937.
(24) Martin, R. H.; Marchant, M. J. *Tetrahedron* **1974**, *30*, 347.

DOI: 10.1021/jacs.6b01303
J. Am. Chem. Soc. 2016, 138, 3587−3595